Published in IET Power Electronics
Received on 13th September 2013
Revised on 28th April 2014
Accepted on 22nd May 2014
doi: 10.1049/iet-pel.2013.0920

ISSN 1755-4535

State observer based sensor less control using Lyapunov's method for boost converters

Hyunki Cho, Sung Jin Yoo, Sangshin Kwak

School of Electrical and Electronics Engineering, Chung-Ang University, Seoul, Korea
E-mail: sskwak@cau.ac.kr

Abstract: This study proposes a state observer based sensorless controller using the Lyapunov's direct method for boost converters. The proposed controller derived from the Lyapunov method considers a large-signal model and the non-linearity of the boost converter, which allows accurate output tracking performance and stability. In addition, a state observer is constructed to estimate the inductor current using an output voltage, an input voltage and a switch control signal. The developed observer enables the proposed controller to be realised with no current sensor for the inductor current, and results in a low cost as well as reliable system free from the noise problem associated with the sensor. The non-linear controller incorporated into the observer is designed with appropriate observer gains determined by linear matrix inequalities. Experimental results are presented to verify the stable operation and output tracking capability for large-signal transients of the proposed sensorless controller based on the Lyapunov method.

1 Introduction

Boost converters have been widely used in various fields such as power conditioning systems with renewable energy sources [1–3], power factor corrections [4–6] and hybrid electric vehicle systems [7, 8]. The feedback-based output voltage control of the boost converter has been considered as one of the most important research areas because accurate voltage regulation with stability under transient conditions is a prerequisite for most applications. Proportional–integral (PI) control methods based on linearised small-signal models in state-space have been widely employed, in which system stability is guaranteed despite of small perturbations at equilibrium points of states. In general, the PI controllers for the boost converter are configured with an outer voltage control loop and an inner current control loop [9–12]. Although the current-mode controllers based on the small-signal models have been popularly employed, the converter with duty cycles over 50% can result in the subharmonic instability when exposed to small-signal disturbance [13]. Control methods using external slope-compensating ramps and predictive current controllers with different modulation techniques have been investigated to solve the subharmonic instability [14]. In addition, large-signal perturbations can substantially derail the tracking response of the converters from the desired values [15, 16]. In order to improve stability of systems with large-signal perturbations, the passivity-based controllers for the boost converter was, through an energy reshaping process, proposed with damping injection [17]. The passivity-based controllers combined with the adaptive control and the sliding mode control have been presented for the boost converters [18, 19]. In addition, the tuning problem for control parameters used for the non-linear passivity-based controllers was addressed [20]. As a part of passivity-based control method, the Lyapunov stability theory has been recently studied to consider intrinsic non-linearity of the dc–dc converters [21–24]. Non-linear control laws derived from Lyapunov's direct method have been proposed for several dc–dc converters such as the buck–boost, boost, Ćuk, buck and multiple-input dc–dc converters [21–23]. The Lyapunov-based controllers exhibit superior output tracking performance and stability over the small-signal-based PI control methods under transient conditions with large-signal perturbations. In addition to the stability issues of the boost converters with large-signal perturbations, sensorless control methods without an inductor current measurement have been proposed to realise low-cost and reliable boost converters. The conventional peak current-mode control method has the disadvantage which is easy to be exposed to the noise from the current sensing process, because the switching occurs at the peak of inductor current. Even if average current-mode control can help to improve the noise robustness, it also needs the Hall effect-based current sensor which is much more expensive than the resistive sensing. In addition, if the dc–dc converter has to supply power in wide load range, the noise performance can be worse while current sensing is carried out in the entire range [25]. A technique for estimating the inductor current using analogue circuits was developed by integrating the inductor voltage, which is obtained from the input/output voltage and switching signals [25]. Furthermore, an estimator for the inductor current was implemented in a digital platform by integrating the inductor voltage using a counter [26].

In this paper, a state observer based sensorless controller using Lyapunov's direct method is proposed for boost converters. A state observer based on the state model of the boost converter is developed to estimate the inductor current using the output voltage, input voltage and switch control signal. The developed state observer enables the realisation of the proposed control system without a current sensor for the inductor current, which results in low cost as well as a reliable system free from the noise problem associated with the sensor, even if the load range of a converter is wide. By considering the non-linearity of the boost converter, the proposed non-linear controller with the observer is designed based on the large-signal model. Thus, accurate output voltage regulation and virtually global stability under transients with large-signal variations are obtained in the proposed control system. In order to achieve appropriate gains for the state observer, this paper utilises the linear matrix inequality (LMI) approach [27–32]. Experimental results are presented to verify the proposed Lyapunov-based controller with the state observer.

2 System dynamic modelling and problem statement

The boost converter is shown in Fig. 1. The input source energy is transferred to the inductor when the switch is turned on. When the switch is off, the input energy, along with the stored inductor energy, is delivered to the output load to obtain the desired output voltage higher than the input voltage.

The dc–dc boost converter based on the switching operation is expressed by the time-averaged state-space large-signal model as [33]

$$\dot{V}_{\mathrm{o}} = -\frac{1}{RC}V_{\mathrm{o}} + \frac{1}{C}(1-u)i_L \tag{1}$$

$$\dot{i}_L = \frac{1}{L}V_s - \frac{1}{L}(1-u)V_{\mathrm{o}} \tag{2}$$

where V_{o}, V_s and i_L represent the average output voltage, the input voltage and the average inductor current during the switching period, respectively. In addition, R, C and L are the load resistance, output capacitance and input inductance, respectively. The continuous duty ratio of the switch is denoted by u, which is confined in $0 \le u \le 1$. From this model, the time-averaged dynamics can be controlled by the continuous duty ratio u, obtained from the controller. The averaged state-space large-signal model in (1) and (2) is then rewritten as

$$\begin{aligned} \dot{\boldsymbol{x}} &= \boldsymbol{A}\boldsymbol{x} + \boldsymbol{B}\boldsymbol{x}u + \boldsymbol{G} \\ y &= \boldsymbol{H}\boldsymbol{x} \end{aligned} \tag{3}$$

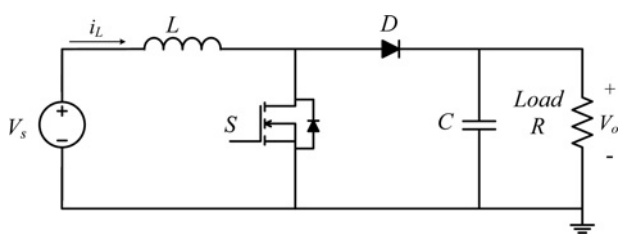

Fig. 1 *DC–DC boost converter topology*

where $\boldsymbol{x} = [V_{\mathrm{o}}, i_L]^{\mathrm{T}}$, $y = V_{\mathrm{o}}$

$$\boldsymbol{A} = \begin{bmatrix} -\frac{1}{RC} & \frac{1}{C} \\ -\frac{1}{L} & 0 \end{bmatrix}, \quad \boldsymbol{B} = \begin{bmatrix} 0 & -\frac{1}{C} \\ \frac{1}{L} & 0 \end{bmatrix},$$

$$\boldsymbol{H} = \begin{bmatrix} 1 & 0 \end{bmatrix}, \quad \boldsymbol{G} = \begin{bmatrix} 0 \\ \frac{V_s}{L} \end{bmatrix}$$

The boost converter should be operated in a manner such that the system state matrix $\boldsymbol{x}$ with the output voltage and the inductor current track the reference matrix $\boldsymbol{x_d} = [V_{\mathrm{ref}}, i_{\mathrm{ref}}]^{\mathrm{T}}$, where V_{ref} and i_{ref} are the reference values of the output voltage and inductor current, respectively. The output reference voltage V_{ref} is determined with the desired transient dynamics by the state response of the first-order low-pass filter as

$$\dot{V}_{\mathrm{ref}} = w_{\mathrm{d}}(V_{\mathrm{cmd}} - V_{\mathrm{ref}}) \tag{4}$$

where V_{cmd} is the command dc output voltage and w_{d} is a constant for the desired transient dynamics of the reference voltage V_{ref}. In order to avoid a sharp voltage command, a first-order low-pass filter is used as the reference model to smooth the desired voltage command. A larger w_{d} forces the reference output voltage V_{ref} to rapidly reach the dc command voltage V_{cmd} at the expense of possible overshoot, whereas all the other signals remain bounded. Based on the system dynamic model of the boost converter, the controller should be designed in such a way that the output voltage follows the desired value with fast transient responses. Moreover, the controller ensures that the boost converter operates under stable conditions, although the boost converter is exposed to large external perturbations such as the step change in the load and the input voltage.

3 Proposed Lyapunov-based non-linear controller with state observer

The overall block diagram of the proposed Lyapunov-based non-linear controller with the state observer is shown in Fig. 2. In the proposed sensorless controller, the observer is designed for accurate estimation of the inductor current i_L using the output voltage V_{o}, input voltage V_s and duty cycle u. The developed observer in the control system can realise the control system without any current sensor and the associated circuitry for inductor current measurement. The output voltage and the input voltage are measured by using the voltage diving of two resistances, and converted to digital signal in the analog-to-digital converter (ADC) block.

A voltage control error is generated between the reference voltage V_{ref} and the estimated output voltage. The inductor reference current i_{ref}, obtained by using the PI controller with voltage error e_v, is compared with the estimated inductor current from the observer to generate the current control error e_i. The non-linear controller generates the duty ratio u for the switch on the basis of the voltage and current control error e_v and e_i. To ensure stability of the entire control system including the state observer, the gains for the observer are determined by solving the inequalities obtained from Lyapunov stability theory using the LMI, taking into consideration the system parameters. Finally, the duty ratio is converted to a switching pulse q using a digital

doi: 10.1049/iet-pel.2013.0920

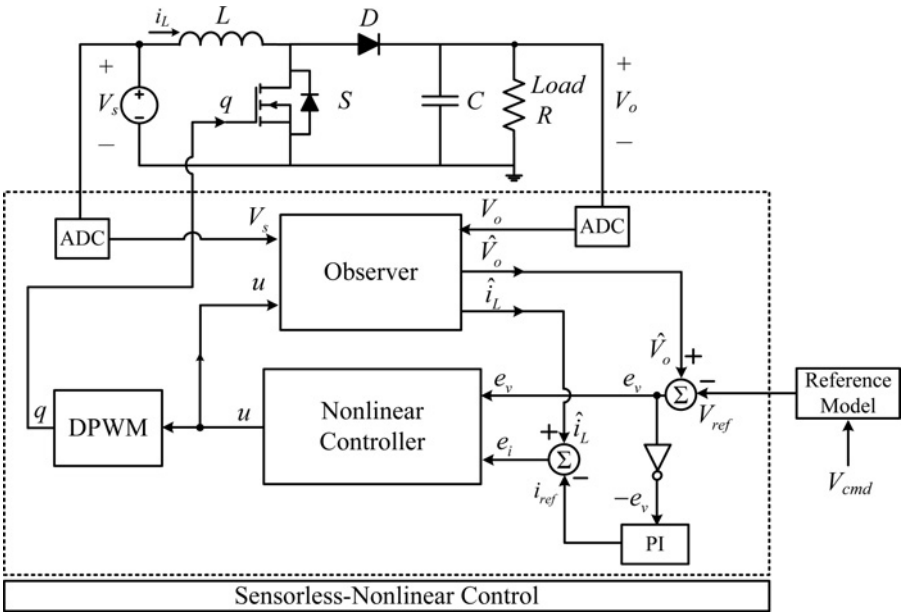

Fig. 2 *Block diagram of the proposed sensorless non-linear control*

pulsewidth modulated (DPWM) block, which compares the high-frequency triangle counter and the duty ratio.

3.1 Observer model design

The state observer is designed to estimate the states of the model, which enables the proposed control system to be realised with no inductor current measurement. The estimated state $\hat{\boldsymbol{x}} = [\hat{V}_o, \hat{i}_L]^T$ is obtained by the state observer, in which the dynamics of the averaged state-space model should behave similar to those of the real model in (3). The observer error between the real and the estimated states is defined as $\tilde{\boldsymbol{x}} = \boldsymbol{x} - \hat{\boldsymbol{x}}$. The proposed observer is represented as

$$\begin{aligned} \dot{\hat{\boldsymbol{x}}} &= \boldsymbol{A}\hat{\boldsymbol{x}} + \boldsymbol{B}\hat{\boldsymbol{x}}u + \boldsymbol{G} + \boldsymbol{F}(y - \hat{y}) \\ \hat{y} &= \boldsymbol{H}\hat{\boldsymbol{x}} \end{aligned} \tag{5}$$

where $\dot{\hat{\boldsymbol{x}}} = [\dot{\hat{V}}_o, \dot{\hat{i}}_L]^T$, $\hat{y} = \hat{V}_o$ and $F = [Fv,\ Fi]^T$ denotes an observer gain matrix. These gains for assuring the stability are chosen by analysing stability of the proposed closed-loop system, which will be presented in Section 3.3.

3.2 Controller design

As shown in Fig. 2, the voltage and current control errors between the reference and the estimated values are represented by defining the control error matrix as $\boldsymbol{e} = [e_v\ e_i]^T$

$$\boldsymbol{e} = \begin{bmatrix} e_v \\ e_i \end{bmatrix} = \begin{bmatrix} \hat{V}_o - V_{ref} \\ \hat{i}_L - i_{ref} \end{bmatrix} \tag{6}$$

The inductor reference current determined by using the PI controller is expressed as $i_{ref} = -(k_P e_v + k_I \int e_v dt)$, where k_P and k_I are given positive constants. The derivative of the control error with respect to time can be represented as follows using (5)

$$\dot{\boldsymbol{e}} = \dot{\hat{\boldsymbol{x}}} - \dot{\boldsymbol{x}}_d = \boldsymbol{A}\hat{\boldsymbol{x}} + \boldsymbol{B}\hat{\boldsymbol{x}}u + \boldsymbol{G} + \boldsymbol{F}(y - \hat{y}) - \dot{\boldsymbol{x}}_d \tag{7}$$

Using the observer model in (5), the proposed controller is determined to stabilise (7) as

$$u = (\boldsymbol{b}^T\boldsymbol{b})^{-1}\boldsymbol{b}^T(-\boldsymbol{K}\boldsymbol{e} - \boldsymbol{A}\boldsymbol{x}_d - \boldsymbol{G} - \boldsymbol{F}(y - \hat{y}) + \dot{\boldsymbol{x}}_d) \tag{8}$$

where $\boldsymbol{b} = \boldsymbol{B}\hat{x}$, the pseudoinverse term $(\boldsymbol{b}^T\boldsymbol{b})^{-1}\boldsymbol{b}^T$ is used and $\boldsymbol{K}$ is a positive definite control gain matrix given as $\boldsymbol{K} = \text{diag}\ \{k_v, k_i\}$. The control gain matrix $\boldsymbol{K}$ is chosen by considering the stability of the system, in the following Section 3.3.

3.3 Stability analysis

Lyapunov's direct method is employed to ensure stability of the controlled system.

Theorem 1: : In the proposed sensorless controller with the observer in (5) and the control law in (8), both the observer and control errors converge to zero, and thus, the controlled closed-loop system is asymptotically stable.

Proof: From (3) and (5), the observer error dynamic is expressed as

$$\dot{\tilde{\boldsymbol{x}}} = (\boldsymbol{A} - \boldsymbol{F}\boldsymbol{H})\tilde{\boldsymbol{x}} + \boldsymbol{B}\tilde{\boldsymbol{x}}u \tag{9}$$

Using (7) and (8), the control error dynamic of the entire control system is represented as

$$\dot{\boldsymbol{e}} = (\boldsymbol{A} - \boldsymbol{K})\boldsymbol{e} \tag{10}$$

A positive definite Lyapunov candidate function, considering both the observer error and the controller error, can be chosen as

$$V = \tilde{\boldsymbol{x}}^T\boldsymbol{P}\tilde{\boldsymbol{x}} + \boldsymbol{e}^T\boldsymbol{e} \tag{11}$$

where $\boldsymbol{P} \in \Re^{2x2}$ is a positive definite matrix. The time derivative of the Lyapunov function V is expressed as

follows using (9) and (10)

$$\begin{aligned}\dot{V} &= \dot{\tilde{\boldsymbol{x}}}^{\mathrm{T}}\boldsymbol{P}\tilde{\boldsymbol{x}} + \tilde{\boldsymbol{x}}^{\mathrm{T}}\boldsymbol{P}\dot{\tilde{\boldsymbol{x}}} + \dot{\boldsymbol{e}}^{\mathrm{T}}\boldsymbol{e} + \boldsymbol{e}^{\mathrm{T}}\dot{\boldsymbol{e}} \\ &= \tilde{\boldsymbol{x}}^{\mathrm{T}}(\boldsymbol{P}(\boldsymbol{A}-\boldsymbol{FH}) + (\boldsymbol{A}-\boldsymbol{FH})^{\mathrm{T}}\boldsymbol{P})\tilde{\boldsymbol{x}} \\ &\quad + 2\tilde{\boldsymbol{x}}^{\mathrm{T}}\boldsymbol{PB}\tilde{\boldsymbol{x}}u + 2\boldsymbol{e}^{\mathrm{T}}(\boldsymbol{A}-\boldsymbol{K})\boldsymbol{e} < 0 \end{aligned} \tag{12}$$

From the inequality $(1/\rho)\cdot\tilde{\boldsymbol{x}}^{\mathrm{T}}\boldsymbol{PBB}^{\mathrm{T}}\boldsymbol{P}\tilde{\boldsymbol{x}} - 2\tilde{\boldsymbol{x}}^{\mathrm{T}}\boldsymbol{PB}\tilde{\boldsymbol{x}}u + \rho u^2\tilde{\boldsymbol{x}}^{\mathrm{T}}\tilde{\boldsymbol{x}} \geq 0$ and $0 \leq u \leq 1$, the second term on the right-hand side of (12) can be

$$\begin{aligned} 2\tilde{\boldsymbol{x}}^{\mathrm{T}}\boldsymbol{PB}\tilde{\boldsymbol{x}}u &\leq \frac{1}{\rho}\tilde{\boldsymbol{x}}^{\mathrm{T}}\boldsymbol{PBB}^{\mathrm{T}}\boldsymbol{P}\tilde{\boldsymbol{x}} + \rho u^2\tilde{\boldsymbol{x}}^{\mathrm{T}}\tilde{\boldsymbol{x}} \\ &\leq \frac{1}{\rho}\tilde{\boldsymbol{x}}^{\mathrm{T}}\boldsymbol{PBB}^{\mathrm{T}}\boldsymbol{P}\tilde{\boldsymbol{x}} + \rho\tilde{\boldsymbol{x}}^{\mathrm{T}}\tilde{\boldsymbol{x}} \end{aligned} \tag{13}$$

where ρ is a positive constant. The derivative of the Lyapunov function in (12) can be, using (13), expressed without the duty cycle u as

$$\begin{aligned}\dot{V} = &\left[\tilde{\boldsymbol{x}}^{\mathrm{T}}\left(\boldsymbol{P}(\boldsymbol{A}-\boldsymbol{FH}) + (\boldsymbol{A}-\boldsymbol{FH})^{\mathrm{T}}\boldsymbol{P} + \frac{1}{\rho}\boldsymbol{PBB}^{\mathrm{T}}\boldsymbol{P} + \rho\boldsymbol{I}\right)\tilde{\boldsymbol{x}}\right] \\ &+ \left[2\boldsymbol{e}^{\mathrm{T}}(\boldsymbol{A}-\boldsymbol{K})\boldsymbol{e}\right] < 0 \end{aligned} \tag{14}$$

where $\boldsymbol{I} \in \Re^{2x2}$ is an identity matrix. □

To make the derivative of the Lyapunov function negative definite, both terms with the square bracket in (14) should be negative, respectively. The observer gain matrix $\boldsymbol{F}$ and the controller gain matrix $\boldsymbol{K}$ are designed in such a way that the respective term with the square bracket in (14) is negative. The former term with the square bracket in (14) becomes negative in the case when the following inequality is satisfied

$$\boldsymbol{P}(\boldsymbol{A}-\boldsymbol{FH}) + (\boldsymbol{A}-\boldsymbol{FH})^{\mathrm{T}}\boldsymbol{P} + \frac{1}{\rho}\boldsymbol{PBB}^{\mathrm{T}}\boldsymbol{P} + \rho\boldsymbol{I} < -\boldsymbol{Q} \tag{15}$$

where $\boldsymbol{Q} \in \Re^{2x2}$ is the positive definite matrix. Therefore the observer gain matrix $\boldsymbol{F}$ can be determined in such a way to satisfy the condition represented as (15).

Remark 1: (Computation of $\boldsymbol{F}$*)*: By employing the Schur complement, the non-LMI of (15) is transformed into a LMI form as [34]

$$\begin{bmatrix} \boldsymbol{PA} + \boldsymbol{A}^{\mathrm{T}}\boldsymbol{P} - \boldsymbol{ZH} - \boldsymbol{H}^{\mathrm{T}}\boldsymbol{Z}^{\mathrm{T}} + \rho\boldsymbol{I} + \boldsymbol{Q} & \boldsymbol{P} \\ \boldsymbol{P} & \rho\boldsymbol{BB}^{\mathrm{T}} \end{bmatrix} < 0 \tag{16}$$

where matrix $\boldsymbol{Z} = \boldsymbol{PF}$.

Although there are no special guidelines for selecting the positive constant ρ, using a considerably high ρ can result in reduced dimensions of the LMIs and more feasible LMIs to obtain the matrix $\boldsymbol{F}$ in (15). With a very high ρ, the inequality (15) can be represented, because the third term of (15) becomes negligible, as

$$\boldsymbol{P}(\boldsymbol{A}-\boldsymbol{FH}) + (\boldsymbol{A}-\boldsymbol{FH})^{\mathrm{T}}\boldsymbol{P} = -\bar{\boldsymbol{Q}} < -(\boldsymbol{Q}+\rho\boldsymbol{I}) \tag{17}$$

where, $\bar{\boldsymbol{Q}}$ is a positive definite matrix satisfying $\bar{\boldsymbol{Q}} > \boldsymbol{Q} + \rho\boldsymbol{I}$ independent of $\boldsymbol{P}$. After selecting the positive constant ρ, the matrices $\boldsymbol{P}$, $\boldsymbol{Q}$ and $\boldsymbol{Z}$ are found by solving the LMIs [35]. As a result, the observer gain matrix $\boldsymbol{F}$ is determined from $\boldsymbol{F} = \boldsymbol{P}^{-1}\boldsymbol{Z}$.

In order to make the latter square bracket term, $2\boldsymbol{e}^{\mathrm{T}}(\boldsymbol{A}-\boldsymbol{K})\boldsymbol{e}$, in (14) negative, the control gain matrix $\boldsymbol{K}$ is chosen so that the matrix $\boldsymbol{A}-\boldsymbol{K}$ becomes a Hurwitz matrix, which implies that all its eigenvalues are strictly located in the left half-plane [36]. Thus, the constants k_v and k_i of the controller gain matrix $\boldsymbol{K}$ are determined as

$$\frac{4}{LC} < \frac{3}{4}\cdot\left(k_v + k_i + \frac{1}{RC}\right)^2 + k_i\cdot\left(k_v + \frac{1}{RC}\right) \tag{18}$$

With the observer gain matrix and the controller gain matrix $\boldsymbol{K}$ to guarantee the negative definite derivative of the Lyapunov function in (14), it can be concluded that the observer and control errors converge to zero as time increases. As a result, the boost converter system with the proposed sensorless controller using the observer is asymptotically stable.

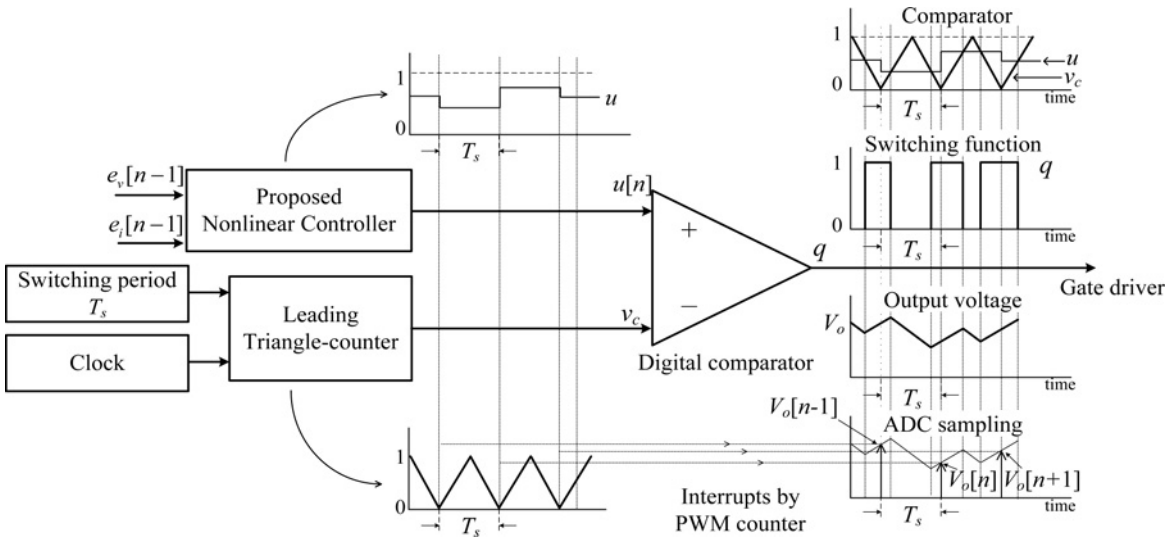

Fig. 3 *Digital implementation of the proposed controller*

doi: 10.1049/iet-pel.2013.0920

Table 1 Experimental parameters for the boost converter controlled by the proposed controller

Experimental parameter	Value
input voltage (V_s)	30 V
output reference dc voltage (V_{cmd})	75 V
switching frequency (f_{sw})	50 kHz
input inductor (L)	587.4 μH
output capacitor (C)	490 μF
load (R)	100 Ω
observer voltage gain (F_v)	4879.5
observer current gain (F_i)	3001.1
controller voltage gain (k_v)	1
controller current gain (k_i)	2275
P gain of PI controller (k_P)	0.016
I gain of PI controller (k_I)	14.912
reference model parameter (w_d)	700
constant (ρ)	$10\,832 \times 10^5$

4 Experimental results

The proposed sensorless-non-linear controller for the boost converter was tested by experiments to verify its tracking capability and stability during large-signal transient conditions. Digital controller of the proposed control algorithm was implemented based on the platform of the average current-mode control [9, 13]. Fig. 3 shows that the digital implementation of the proposed controller by using the DPWM and ADC in the digital signal processor (DSP). The proposed non-linear controller generates the duty ratio $u[n]$ in each switching period by using the voltage and the current tracking errors, e_v $[n–1]$ and e_i $[n–1]$. At every switching period, the counter produces interrupting signals to trigger the ADC block for the analogue to digital conversion of the output voltage. The leading triangle counter with the average current mode was used in this experiment to assure the stability for the entire values of the duty cycle [13]. The switching pulse q is generated by comparing the duty ratio with the counter v_c, and transmitted to the gate driver.

In this paper, a converter is designated to be applied to an application of the fuel cell generation as referred [37]. In order to show the design consideration, the circuit parameters, input/output conditions and gains used for the experiments

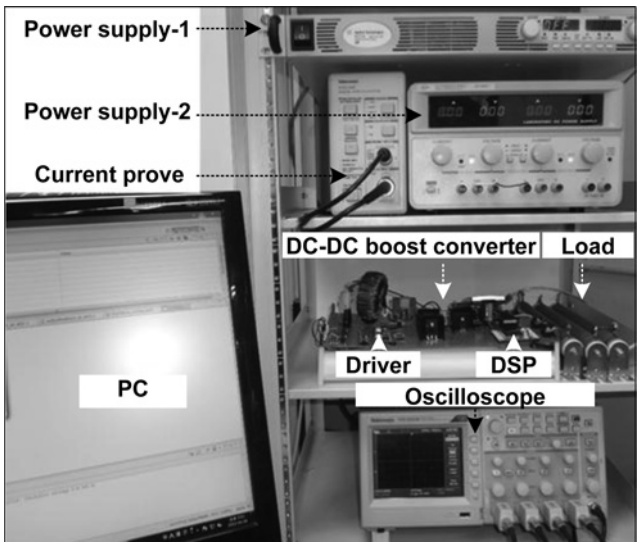

Fig. 4 *Experiment set of prototype dc–dc boost converter with the proposed controller*

are specified in Table 1. By selecting 0.02 V and 620 mA for the output voltage ripple and inductor current ripple, respectively, inductor and output capacitor are determined with $L = 587.4$ μH and capacitor $C = 490$ μF with specifications of $V_s = 30$ V, $V_{ref} = 75$ V, $f_{sw} = 50$ kHz and load variations between 80 and 150 Ω [38].

A prototype of the boost converter was fabricated, as shown in Fig. 4, with an International Rectifier power metal oxide semiconductor field effect transistor (MOSFET) (IRFP22N60 K) with 600 V/22 A, a Sanken electric diode (FMG-22S) and an optocoupler (HCPL-3140) as the gate drivers. In addition, the proposed controller was implemented with a Texas Instrument DSP TMS320F28335. The PI gains were selected to obtain the inductor current reference i_{ref}. The observer gains F_v and F_i were determined in (16) by using chosen $\rho = 10\,832 \times 10^5$ and the LMI tool in MATLAB. The controller gains in matrix $\boldsymbol{K}$ were set in such a way that $(4/LC) < 0.75 \cdot [k_v + k_i + (1/RC)]^2 + k_i \cdot [k_v + (1/RC)]$ for obtaining a Hurwitz matrix $(\boldsymbol{A}–\boldsymbol{K})$ in (14), which implies stable conditions. A simple PI

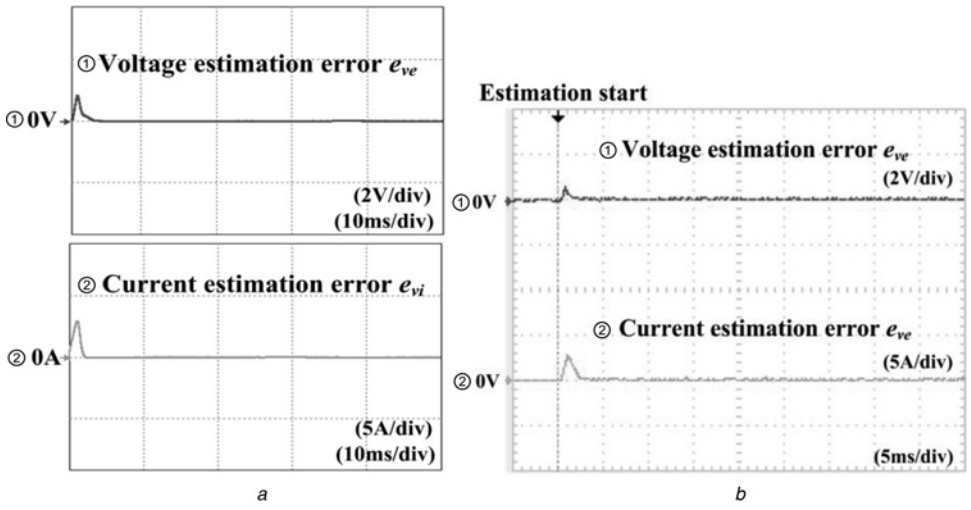

Fig. 5 *Results of the simulation and the experiment*

a Simulation results

b Experiment results for verifying states estimation: ① voltage estimation error $e_{ve} = (V_o - \hat{V}_o)$ and ② current estimation error $e_{ie} = (I_L - \hat{I}_L)$

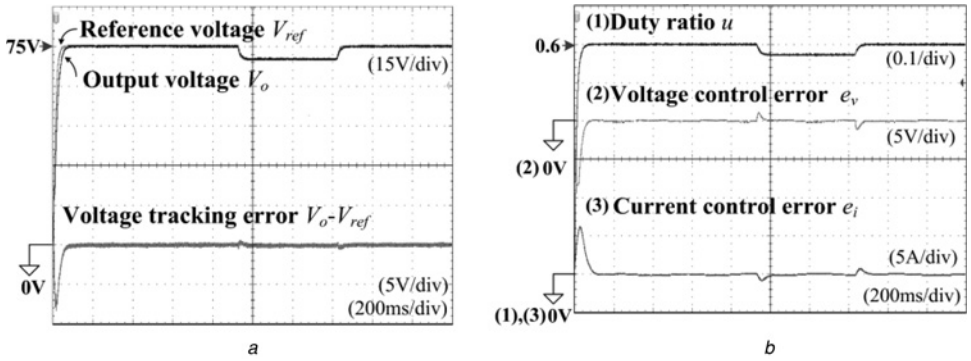

Fig. 6 *Experimental results for condition 1*

a Voltage response V_o, V_{ref} and voltage tracking error ($V_o - V_{ref}$)
b Duty ratio u, voltage control error e_v and current control error e_i

controller was used for deciding the desired inductor current reference from the voltage tracking error e_v, where the transient performance and the stability margin depend on the gains of the PI controller [39]. Fig. 5 shows the results of the simulation and the experiment to verify the accuracy of states estimation. Fig. 5*a* is simulation result, where voltage and current estimation error is defined as e_{ve} and e_{vi}, respectively. When the estimation starts in the observer, there are instant errors of voltage and current estimation which are quickly decreased to zero during the estimation process. Results of the estimation in the experiment shown in Fig. 5*b* seem to be similar with the simulation results, but the experimental results have noticeable noise which is generated in the digital to analogue (DAC) converting process. The DAC process is implemented to show the estimation result in the DSP as an analogue signal.

The experimental results to demonstrate the stability of the proposed sensorless-non-linear controller are shown under transient conditions specified as follows:

Condition 1: Startup transient and step change in the reference voltage V_{ref} between 75 and 70 V.
Condition 2: Startup transient and step change in the reference voltage V_{ref} between 75 and 80 V.
Condition 3: Step change in the input voltage V_s between 30 and 25 V.
Condition 4: Step change in the input voltage V_s between 30 and 35 V.
Condition 5: Step change in the load R between 100 and 150 Ω; the load current varies from 750 to 500 mA.
Condition 6: Step change in the load R between 100 and 80 Ω; the load current varies from 750 to 938 mA.

Figs. 6 and 7 show the experimental results for conditions 1 and 2, respectively. From Figs. 6*a* and 7*a*, it is seen that the output voltages trace their reference, and the voltage tracking errors become zero within 56 ms after the start-up transient and within 50 ms after the step change in the reference voltage. The proposed controller creates a duty ratio so that the control errors diminish after the transient conditions, as shown in Figs. 6*b* and 7*b*. Therefore the boost converter controlled by the proposed controller can achieve output voltage tracking capability with no serious overshoot and no long settling time for startup and reference voltage transients.

The step changes in the input voltage for conditions 3 and 4 are tested (Figs. 8 and 9), where the input voltage undergoes a change of typically 17% of the nominal value. In Figs. 8*a* and 9*a*, the output voltage and tracking error show that the converter controlled by the proposed control algorithm has good output voltage tracking performance with stable operation for varying input voltage conditions. The output voltage is regulated for stable operation with only a temporary increase in the control errors, as shown in Figs. 8*b* and 9*b*.

Figs. 10 and 11 show the performance of the boost converter operated by the proposed controller for step changes in the load for conditions 5 and 6, respectively. It results in the load current variation, respectively, from 750 to 500 mA in the condition 5 and from 750 to 938 mA in the condition 6. In Figs. 10*a* and 11*a*, the output voltage responses show that the output voltage with respect to each of the conditions slightly increases or decreases with the step change in the load current during the load transient;

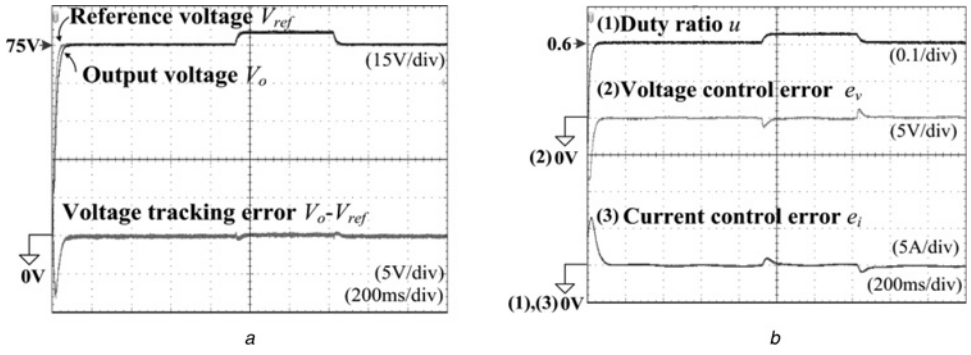

Fig. 7 *Experimental results for condition 2*

a Voltage response V_o, V_{ref} and voltage tracking error ($V_o - V_{ref}$)
b Duty ratio u, voltage control error e_v and current control error e_i

doi: 10.1049/iet-pel.2013.0920

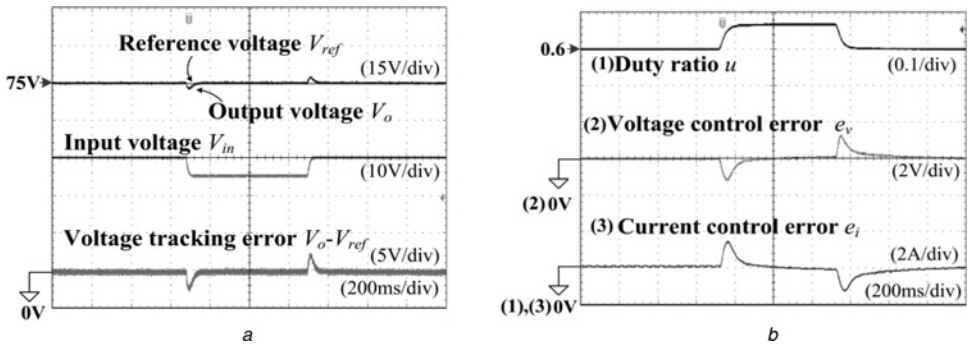

Fig. 8 *Experimental results for condition 3*

a Voltage response V_o, V_{ref}, input voltage V_s and voltage tracking error ($V_o - V_{ref}$)
b Duty ratio u, voltage control error e_v and current control error e_i

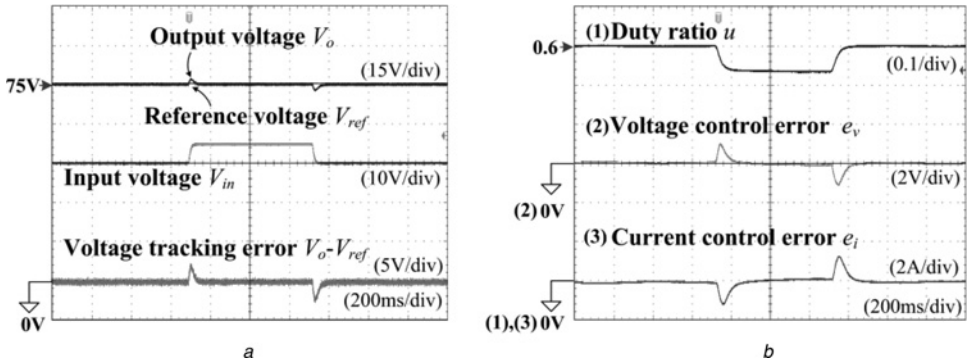

Fig. 9 *Experimental results for condition 4*

a Voltage response V_o, V_{ref}, input voltage V_s and voltage tracking error ($V_o - V_{ref}$)
b Duty ratio u, voltage control error e_v and current control error e_i

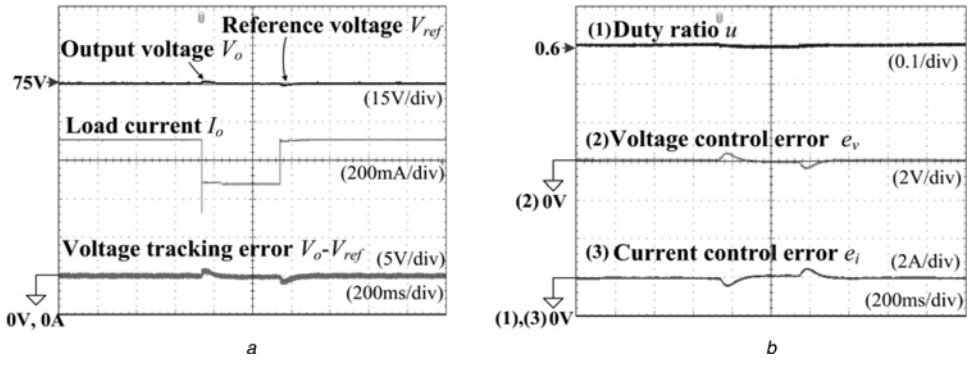

Fig. 10 *Experimental results for condition 5*

a Voltage response V_o, V_{ref}, load current I_o and voltage tracking error (V_o–V_{ref})
b Duty ratio u, voltage control error e_v and current control error e_i

however, it immediately converges to the desired output voltage. Moreover, e_v and e_i also drop to zero.

This paper compares the proposed state observer based sensorless-non-linear controller with the conventional PI controller, in terms of the mean-square error (MSE), the peak overshoot, the settling time and the recovery time. The MSE defined as (19) is employed to compare the output voltage tracking capability [37]

$$\mathrm{MSE} = \frac{1}{T}\sum_{n=1}^{T} e_v^2(n) \tag{19}$$

where n and T is the sampling point and the total number of the sampling points, respectively.

The comparison results for the start-up and the reference voltage changes are summarised in Table 2. The settling time in this comparison is defined as 2% error band of a steady-state value of the output voltage. The MSEs resulted from the proposed controller is reduced by over 26% in comparison with the conventional PI controller, as shown in Table 2, which implies that the voltage tracking capability of the proposed method is considerably improved. Furthermore, the boost converter operated with the proposed controller shows no overshoot under the start-up and reference voltage

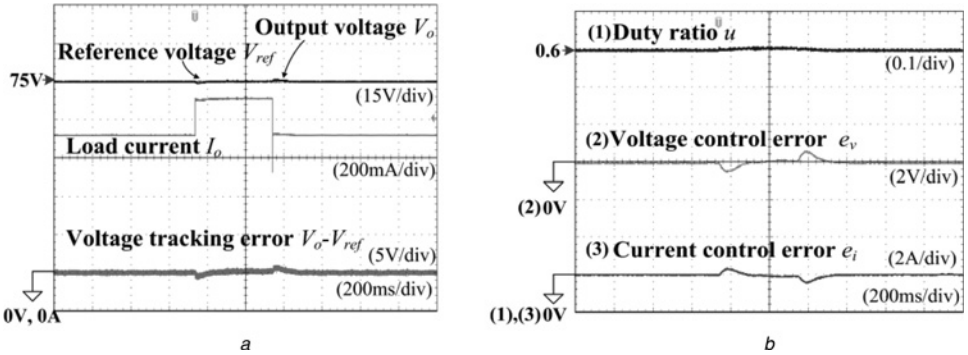

Fig. 11 *Experimental results for condition 6*

a Voltage response V_o, V_{ref}, load current I_o and voltage tracking error ($V_o - V_{ref}$)
b Duty ratio u, voltage control error e_v and current control error e_i

Table 2 Performance comparisons of the proposed controller and the conventional PI controller in the conditions 1 and 2

Test conditions	Performances									
	MSE		Overshoot, V				Settling time, ms			
	Proposed	PI	Proposed		PI		Proposed		PI	
			Start-up	V_{ref} step change	Start-up	V_{ref} step change	Start-up	V_{ref} step change	Start-up	V_{ref} step change
condition 1	0.886	1.200	no overshoot	1.1	2.3	2.2	14.0	6.0	14.8	6.6
condition 2	0.891	1.212	no overshoot	1.2	2.4	2.3	14.0	6.2	14.8	7.3

Table 3 Performance comparisons of the proposed controller and the conventional PI controller in the conditions from 3 to 6

Test conditions	Performances					
	MSE		Overshoot, V		Recovery time, ms	
	Proposed	PI	Proposed	PI	Proposed	PI
condition 3	0.611	0.612	2.431	2.436	83.2	83.6
condition 4	0.571	0.573	2.203	2.209	83.6	84.2
condition 5	0.434	0.625	1.303	2.061	80.3	157.4
condition 6	0.427	0.587	1.123	1.724	28	95.1

transient. With regards of the settling time, the proposed controller is slightly faster than the PI controller.

Table 3 illustrates the performance comparisons with step changes of the input voltage and the load, where the recovery time is utilised to compare how fast the output voltage traces its reference under step changes of the input voltage and the load. It is seen that while it leads to slightly better performance for the step change of the input voltage, the proposed controller yields superior results in comparison with the conventional method with the load-step change. The proposed method shows 27 and 34% reduction in the MSE and the peak overshoot under the step changes of the load, respectively. Moreover, the output voltage faster traces the reference by 48% with the load-step change, compared with the conventional PI controller.

5 Conclusion

In this paper, a sensorless controller with a state observer has been proposed using Lyapunov's direct method for boost converters. The proposed controller was designed with large-signal model stability on the basis of the Lyapunov stability theorem to obtain output voltage tracking capability with large-signal stability for large-signal perturbations. In addition, a state observer was constructed to estimate the inductor current using the output voltage, input voltage and switch control signal. The experimental results verified the stable operation and output tracking capability of the proposed sensorless controller for large-signal transients based on the Lyapunov method.

6 Acknowledgments

This work was supported by the National Research Foundation of Korea (NRF) grant funded by the Korean government (MSIP) (2014R1A2A2A01006684) and the Chung-Ang University Exellent Student Scholarship.

doi: 10.1049/iet-pel.2013.0920

7 References

1 Lin, B.R., Dong, J.Y.: 'New zero-voltage switching DC–DC converter for renewable energy conversion systems', *IET Power Electron.*, 2011, **5**, (4), pp. 393–400
2 Sharma, R., Rasmussen, T.W., Jensen, B.B.: 'Application of a synchronous generator with a boost converter in wind turbines: an experimental overview', *IET Power Electron.*, 2012, **6**, (6), pp. 414–423
3 Li, W., He, X.: 'Review of nonisolated high-step-up DC/DC converters in photovoltaic grid-connected applications', *IEEE Trans. Ind. Electron.*, 2011, **58**, (4), pp. 1239–1250
4 Genc, N., Iskender, I.: 'DSP-based current sharing of average current controlled two-cell interleaved boost power factor correction converter', *IET Power Electron.*, 2011, **4**, (9), pp. 1015–1022
5 Roggia, L., Beltrame, F., Eduardo Baggio, J., Renes Pinheiro, J.: 'Digital current controllers applied to the boost power factor correction converter with load variation', *IET Power Electron.*, 2012, **5**, (5), pp. 532–541
6 Musavi, F., Edington, M., Eberle, W., Dunford, W.G.: 'Control loop design for a PFC boost converter with ripple steering', *IEEE Trans. Ind. Appl.*, 2013, **49**, (1), pp. 118–126
7 Tani, A., Camara, M.B., Dakyo, B.: 'Energy management based on frequency approach for hybrid electric vehicle applications: fuel-cell/lithium-battery and ultracapacitors', *IEEE Trans. Veh. Technol.*, 2012, **61**, (8), pp. 3375–3386
8 Mazumder, S.K., Jedraszczak, P.: 'Evaluation of a SiC dc/dc converter for plug-in hybrid-electric-vehicle at high inlet-coolant temperature', *IET Power Electron.*, 2010, **4**, (6), pp. 708–714
9 Chattopadhyay, S., Das, S.: 'A digital current-mode control technique for dc–dc converters', *IEEE Trans. Power Electron.*, 2006, **21**, (6), pp. 1718–1726
10 Kondrath, N., Kazimierczuk, M.K.: 'Control current and relative stability of peak current-mode controlled pulse-width modulated dc–dc converters without slope compensation', *IET Power Electron.*, 2009, **3**, (6), pp. 936–946
11 Cho, B.H., Bae, H.S., Lee, J.H.: 'Review of current mode control schemes and introduction of a new digital current mode control method for the parallel module dc–dc converters'. Proc. Power Electronics and Motion Control Conf., 2009, pp. 202–210
12 Leyva-Ramos, J., Ortiz-Lopez, M.G., Diaz-Saldierna, L.H., Martinez-Cruz, M.: 'Average current controlled switching regulators with cascade boost converters', *IET Power Electron.*, 2011, **4**, (1), pp. 1–10
13 Jingquan, C., Prodic, A., Erickson, R.W., Maksimovic, D.: 'Predictive digital current programmed control', *IEEE Trans. Power Electron.*, 2003, **18**, (1), pp. 411–419
14 Yang, C.C., Wang, C.Y., Kuo, T.H.: 'Current-mode converters with adjustable-slope compensating ramp'. Proc. IEEE Asia Pacific Conf. on Circuits and Systems (APCCAS), 2006, pp. 654–657
15 Mattavelli, P.: 'Digital control of dc–dc boost converters with inductor current estimation'. Proc. Applied Power Electronics Conf. (APEC), 2004, pp. 74–80
16 Zafrany, I., Ben-Yaakov, S.: 'A chaos model of subharmonic oscillations in current mode PWM boost converters'. Proc. IEEE Power Electronics Specialist Conf. (PESC), 1995, pp. 1111–1117
17 Sira-Ramirez, H., Ortega, R.: 'Passivity-based controllers for the stabilization of DC-to-DC power converters'. Proc. 34th IEEE Conf. on Decision & Control, 1995, pp. 3471–3475
18 Seleme Jr. S.I., Rosa, A.H.R., Morais, L.M.F., Donoso-Garcia, P.F., Cortizo, P.C.: 'Evaluation of adaptive passivity-based controller for power factor correction using a boost converter', *IET Power Electron.*, 2012, **6**, (14), pp. 2168–2178
19 Escobar, G., Sira-Ramirez, H.: 'A passivity based-sliding mode control approach for the regulation of power factor precompensators'. Proc. 37th IEEE Conf. on Decision & Control, 1998, pp. 2423–2424
20 Jeltsema, D., Scherpen, J.M.A.: 'Tuning of passivity-preserving controllers for switched-mode power converters', *IEEE Trans. Autom. Control*, 2004, **49**, (8), pp. 1333–1343
21 Kawasaki, N., Nomura, H., Masuhiro, M.: 'A new control law of bilinear DC–DC converters developed by direct application of Lyapunov', *IEEE Trans. Power Electron.*, 1995, **10**, (3), pp. 318–325
22 Wei, Z., Bao-bin, L.: 'Analysis and design of DC–DC buck converter with nonlinear adaptive control'. Proc. Int. Conf. on Computer Science & Education (ICCSE), 2012, pp. 1036–1038
23 Onwchekwa, C.N., Kwasinski, A.: 'Analysis of boundary control for a multiple-input DC–DC converter topology'. Proc. Applied Power Electronics Conf. (APEC), 2011, pp. 1232–1237
24 Berkovich, Y., Ioinovici, A.: 'Large-signal stability-oriented design of boost regulators based on a Lyapunov criterion with nonlinear integral', *IEEE Trans. Circuits Syst. I*, 2002, **49**, (11), pp. 1610–1619
25 Midya, P., Krein, P.T., Greuel, M.F.: 'Sensorless current mode control – an observer-based technique for DC–DC converters', *IEEE Trans. Power Electron.*, 2001, **16**, (4), pp. 522–526
26 Trescases, O., Parayandeh, A., Prodic, A., Tung Ng, W.: 'Sensorless digital peak current controller for low-power DC–DC SMPS based on a bi-directional delay line'. Proc. IEEE Power Electronics Specialist Conf. (PESC), 2007, pp. 1670–1676
27 Tingshu, H.: 'A nonlinear-system approach to analysis and design of power-electronic converters with saturation and bilinear terms', *IEEE Trans. Power Electron.*, 2011, **26**, (2), pp. 399–410
28 Olalla, C., Leyva, R., El Aroudi, A., Garcés, P., Queinnec, I.: 'LMI robust control design for boost PWM converters', *IET Power Electron.*, 2008, **3**, (1), pp. 75–85
29 Lian, K.Y., Liou, J.J.: 'Output tracking control for fuzzy systems via output feedback design', *IEEE Trans. Fuzzy Syst.*, 2006, **14**, (5), pp. 628–639
30 Hasegawa, M.: 'Robust-adaptive-observer design based on γ-positive real problem for sensorless induction-motor drives', *IEEE Trans. Ind. Electron.*, 2006, **53**, (1), pp. 76–85
31 Martínez-Salamero, L., García, G., Orellana, M., *et al.*: 'Analysis and design of a sliding-mode strategy for start-up control and voltage regulation in a buck converter', *IET Power Electron.*, 2013, **6**, (1), pp. 52–59
32 Lan, Y.H., Huang, H.X., Zhou, Y.: 'Observer-based robust control of a $(1 \leq a < 2)$ fractional-order uncertain systems: a linear matrix inequality approach', *IET Control Theory Applic.*, 2012, **6**, (2), pp. 229–234
33 Middlebrook, R.D., Ćuk, S.: 'A general unified approach to modeling switching-converter power stages'. Proc. IEEE Power Electronics Specialist Conf. (PESC), 1976, pp. 18–34
34 Lian, K.-Y., Chiang, C.-H., Tu, H.-W.: 'LMI-based sensorless control of permanent-magnet synchronous motors', *IEEE Trans. Ind. Electron.*, 2007, **54**, (5), pp. 2769–2778
35 Chen, C.T.: 'Linear system theory and design' (Oxford University Press, New York, 1999)
36 Slotine, J.-J.E., Li, W.: 'Applied nonlinear control' (Prentice-Hall, Englewood Cliffs, NJ, 1991)
37 Wai, R.-J., Shih, L.-C.: 'Adaptive fuzzy-neural-network design for voltage tracking control of a DC–DC boost converter', *IEEE Trans. Power Electron.*, 2012, **27**, (4), pp. 2104–2115
38 Mohan, N., Undeland, T.M., Robbins, W.: 'Power electronics: converters, applications, and design' (Media Enhanced, John Wiley & Sons, Inc., 2003, 3rd edn.)
39 Khalil, H.K.: 'Nonlinear systems' (Prentice-Hall, Upper Saddle River, NJ, 1996)